Biointerphases
A Journal of Biomaterials and Biological Interfaces

Cellular interactions with polystyrene nanoplastics—The role of particle size and protein corona

Cite as: Biointerphases **16**, 041001 (2021); https://doi.org/10.1116/6.0001124
Submitted: 06 May 2021 • Accepted: 15 June 2021 • Published Online: 08 July 2021

Shinji Kihara, Alexander Ashenden, Manmeet Kaur, et al.

Biointerphases
A Journal of Biomaterials and Biological Interfaces

ARTICLE

avs.scitation.org/journal/bip

Cellular interactions with polystyrene nanoplastics—The role of particle size and protein corona

Cite as: Biointerphases 16, 041001 (2021); doi: 10.1116/6.0001124
Submitted: 6 May 2021 · Accepted: 15 June 2021 ·
Published Online: 8 July 2021

Shinji Kihara,[1,2,a)] Alexander Ashenden,[3] Manmeet Kaur,[4] Judith Glasson,[4] Sunandita Ghosh,[1,2] Nadine van der Heijden,[1,2,5] Anna E. S. Brooks,[6,7] Jitendra P. Mata,[8] Stephen Holt,[8] Laura J. Domigan,[2,4] Ingo Köper,[3] and Duncan J. McGillivray[1,2]

AFFILIATIONS

[1]School of Chemical Sciences, The University of Auckland, Auckland 1010, New Zealand
[2]The MacDiarmid Institute for Advanced Materials and Nanotechnology, Wellington 6140, New Zealand
[3]Institute for Nanoscale Science and Technology, College for Science and Engineering, Flinders University, Adelaide, SA 5042, Australia
[4]Department of Chemical and Materials Engineering, The University of Auckland, Auckland 92019, New Zealand
[5]Julius Institute, Department of Physics, Utrecht University, Leuvenlaan 4, 3584CE Utrecht, The Netherlands
[6]School of Biological Sciences, The University of Auckland, Auckland 1010, New Zealand
[7]Maurice Wilkins Centre for Molecular Biodiscovery, The University of Auckland, Auckland 0632, New Zealand
[8]Australian Centre for Neutron Scattering, Australian Nuclear Science and Technology Organisation, Locked Bag 2001, Kirrawee DC, Sydney, NSW 2232, Australia

[a)]Author to whom correspondence should be addressed: shinji.kihara@auckland.ac.nz

ABSTRACT

Plastic waste is ubiquitously spread across the world and its smaller analogs—microplastics and nanoplastics—raise particular health concerns. While biological impacts of microplastics and nanoplastics have been actively studied, the chemical and biological bases for the adverse effects are sought after. This work explores contributory factors by combining results from *in vitro* and model mammalian membrane experimentation to assess the outcome of cell/nanoplastic interactions in molecular detail, inspecting the individual contribution of nanoplastics and different types of protein coronae. The *in vitro* study showed mild cytotoxicity and cellular uptake of polystyrene (PS) nanoplastics, with no clear trend based on nanoplastic size (20 and 200 nm) or surface charge. In contrast, a nanoplastic size-dependency on bilayer disruption was observed in the model system. This suggests that membrane disruption resulting from direct interaction with PS nanoplastics has little correlation with cytotoxicity. Furthermore, the level of bilayer disruption was found to be limited to the hydrophilic headgroup, indicating that transmembrane diffusion was an unlikely pathway for cellular uptake—endocytosis is the viable mechanism. In rare cases, small PS nanoplastics (20 nm) were found in the vicinity of chromosomes without a nuclear membrane surrounding them; however, this was not observed for larger PS nanoplastics (200 nm). We hypothesize that the nanoplastics can interact with chromosomes prior to nuclear membrane formation. Overall, precoating PS particles with protein coronae reduced the cytotoxicity, irrespective of the corona type. When comparing the two types, the extent of reduction was more apparent with soft than hard corona.

I. INTRODUCTION

Microplastic and nanoplastic contamination is a modern societal challenge, resulting from the combination of mass production of plastics and their highly resistant nature.[1,2] Nanoplastics (<1000 nm in size) are easily ignored as they are visually less impactful than bulk- and microplastics, although their small sizes facilitate their entry into biological systems.[3] Major international reports[4–7] have identified nanoplastics as a vital area of research, urging the increase in their study to overcome the significant knowledge gap.

An increasing number of articles in recent years have reported the adverse effects nanoplastics can cause to marine organisms,[8–10] and discussions surrounding their implications to human health have begun.[9,11–13] Specific effects vary from species to species[14]—examples include impaired reproduction,[15–17] malformation of body parts,[15] behavioral effects,[15,18] and transgenerational effects.[17] Nanoplastics have also been found to bioaccumulate and propagate through the food chain.[15] As the adverse effects on model organisms are actively explored, reports on *in vitro* experiments[19,20] have sought the mechanism causing these physiological effects. Identifying the toxicological mechanism is complex as multiple factors contribute to it.

An understanding of the biological activity of nanoplastics can be gained from nanotoxicology. Toxicological mechanisms can be explored by establishing causal relationships between the properties of the nanoplastic particles, underlying biochemical processes, and physiological effects.[21] One main challenge is that the surface characteristics of the nanoplastic particles are altered upon contact with biological fluids. A well-known example is the protein corona,[19,22] where protein molecules surround the nanoplastic surface forming coronalike complex structures. Because of this surface alteration, the particles acquire a new biointerface,[23] different from the pristine nanoparticles. Indeed, the presence of a protein corona significantly affects the biological outcomes of the nanoparticles, including cellular interactions[24,25] and immunological responses.[26] Furthermore, addressing the causation of biochemical processes requires knowledge of the molecular details of biological entities involved in each event to correctly understand their relationship to the biological outcome. Such aspects have been infrequently discussed or experimentally studied for nanoparticles in general and less so for nanoplastics.

In our early work,[22] we illustrated a model system, where polystyrene (PS) nanoplastics were surrounded by either a soft or hard protein corona (the two major structural regimes) of human serum albumin (HSA). The structures of both coronae were then resolved using neutron scattering. Due to the attractive electrostatic interactions holding it together, the hard corona has a tendency to form colloidal aggregates, best described as a fractal structure. Interestingly, the proteins that participate in the soft corona exhibit enhanced intramolecular interactions (in comparison to the native polystyrene and HSA), which may or may not affect subsequent cellular interactions. We also demonstrated that soft and hard corona formation can be controlled by modifying the surface charges of the components. Applying this theory, this work uses net positive lysozyme (LYS) as well as HSA (net negative) as model corona proteins, allowing to create opposite types of protein corona without changing the type of PS particles. A detailed account of HSA and LYS soft and hard coronae formation and structure is documented elsewhere.[22,27] With this, we are able to explore the particle and protein effect independently.

The present work concerns the relationship between nanoplastic properties in conjunction with different types of protein coronae and cellular responses. To investigate the link between the two, we approached the study from two different perspectives. The first approach uses an *in vitro* experiment with human alveolar epithelial (A549) cells, studying the cytotoxicity, cell damage, and cellular uptake, all of which correlate with the observed adverse physiological effects. Since this work attempts to establish the relationship between model protein corona structure and the biological outcome, proteins present in culture media are removed prior to adding the nanoplastic/corona complex (or without protein corona). The physical properties of nanoplastics have been investigated, and conditions at which the soft or hard coronae form are established in our previous work (a summary is listed in Table I).

The second approach employs a model tethered lipid bilayer 1-palmitoyl-2-oleoyl-glycero-3-phosphocholine (POPC) in combination with cholesterol, tethered to 2,3-di-*O*-phytanyl-*sn*-glycerin-1-tetraethylenglycol lipoic acid ester (DPhyTL) with β-mercaptoethanol (β-ME). This formulation of tethered lipid bilayer mimics the mammalian cell membrane and enables investigation with the molecular details of interactions between nanoplastics (and nanoplastic/protein corona complex) and the cell membrane. A tethered bilayer was chosen as anchored lipids simulate the realistic, fluid nature of a cell membrane, as opposed to the conventionally used supported

TABLE I. Summary of the physical characteristics of PS nanoplastics and PS/protein corona complexes. The primary PS particle diameter, composite particle size, and shape were determined by small-angle neutron scattering (SANS), and hydrodynamic diameter was estimated by dynamic light scattering (DLS) in our previous work.[22,31]

	Primary PS particle diameter (SANS)/nm	Composite particle size (SANS)/nm	Shape (SANS)	Hydrodynamic diameter (DLS)/nm
PS(−)small	22.6 (±1.0)	N/A	Spherical	32 (PDI = 0.1)
PS(−)small/HSA Soft corona		27.0 (fixed)	Core-shell like sphere	34 (PDI = 0.09)
PS(−)small/LYS Hard corona		5980 (±250)	Fractal aggregate	>5000 (PDI = 1.0)
PS(+)small	22.2 (±1.0)	N/A	Spherical	39 (PDI = 0.11)
PS(+)small/HSA Hard corona		1110 (±335)	Fractal aggregate	>5000 (PDI = 1.0)
PS(+)small/LYS Soft corona		27.4 (fixed)	Core-shell like sphere	42 (PDI = 0.1)
PS(−)large	222 (±0.1)	N/A	Spherical	226 (PDI = 0.02)
PS(−)large/HSA Soft corona		226 (fixed)	Core-shell like sphere	230 (PDI = 0.02)
PS(−)large/LYS Hard corona		9450 (±213)	Fractal aggregate	>5000 (PDI = 1.0)
PS(+)large	217 (±0.1)	N/A	Spherical	229 (PDI = 0.01)
PS(+)large/HSA Hard corona		~8500 (±1600)	Pearl neckless chain (fractal)	315 (PDI = 0.02)
PS(+)large/LYS Soft corona		220 (fixed)	Core-shell like sphere	236 (PDI = 0.02)

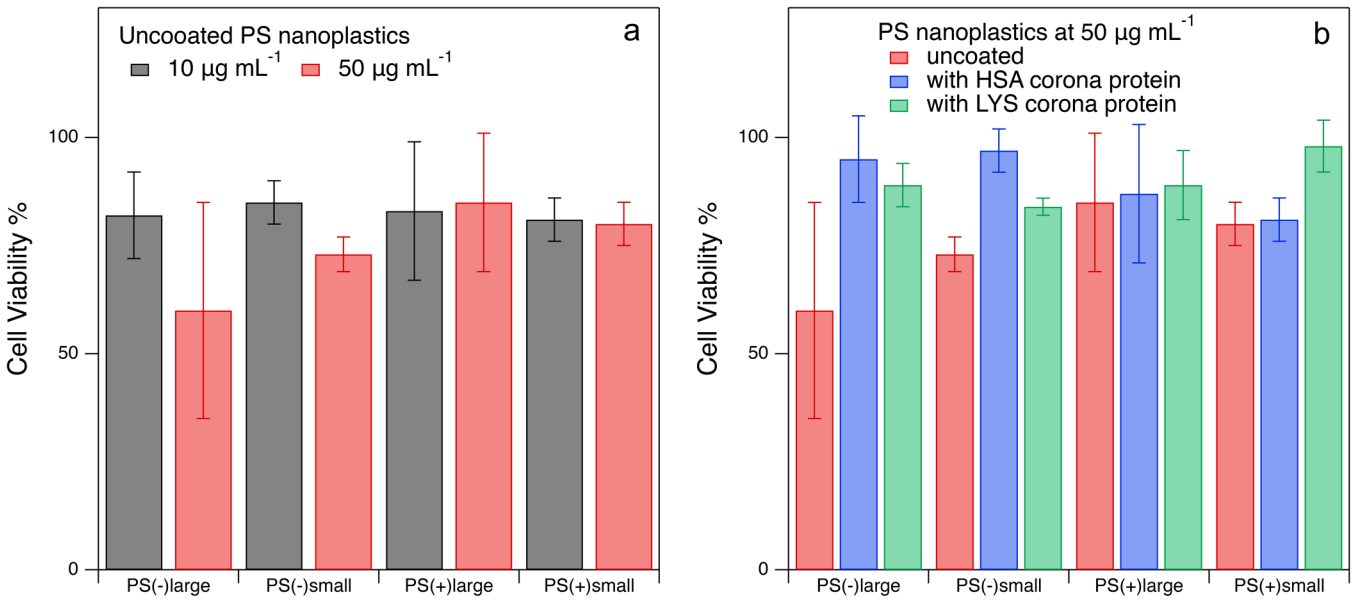

FIG. 1. Summary of MTT cytotoxicity assay using A549 cells. The cell viability % is shown for the A549 cells exposed to two concentrations of uncoated PS nanoplastics (left) and the ones exposed to a fixed concentration of PS (50 μg ml^{-1}) and HSA or LYS corona protein at 15 μg ml^{-1} (right). The results are the average of triplicate and the error is shown inside the parentheses.

lipid bilayer which may be limited by its rigid nature.[28] A detailed characterization of the tethered lipid bilayer can be found elsewhere.[28–30] We evaluate the membrane stability using electrochemical impedance spectroscopy (EIS) and assess the membrane structural integrity at the nanometer resolution using neutron reflectometry (NR).

The structural aspects of soft and hard coronae, as well as the different properties of nanoplastics, are considered in the critical evaluation of correlation/causation relationships. In particular, this work explores the effect of nanoplastic surface (denoted "–" or "+") charges and sizes. Namely, four PS nanoplastics were used, PS(−)small and PS(+)small representing small PS nanoplastics (20 nm diameter) and PS(−)large and PS(+)large, which are sized ∼200 nm. Our structural characterization[22] concluded that the hard protein corona is created when nanoplastics and proteins carry opposite charges, while the same charges lead to soft protein corona formation. To this end, this work illustrates a molecular understanding of membrane damage caused in the absence (uncoated PS) and presence of hard and soft coronae (coated PS), which may explain some of the toxicological effects observed *in vitro*.

II. RESULTS

A. *In vitro* cellular interactions with PS nanoplastics and PS/protein corona complexes

A549 cells were tested for 3-[4,5-dimethylthiazole-2-yl]-2,5-diphenyltetrazolium bromide (MTT) assay to investigate the cytotoxicity of PS nanoplastics and PS/protein corona complexes. First, bare PS nanoplastics, with different sizes and charges, were introduced to confluent cell monolayers at concentrations of 50 and 10 μg ml^{-1} (typical concentrations tested in the literature).[24,25] At both concentrations, mild cytotoxicity was observed, although there were no clear size and/or charge related trends observed (at $p < 0.05$ significant level obtained by two-tailed t-test, Fig. 1 and Table II). When the proteins (15 μg ml^{-1}, approximately covering the surface area of PSsmall) were introduced to the PS nanoplastics, cytotoxicity was mitigated to <10% cell death, and for the PS(+)small/LYS soft corona, the cytotoxic effect of PS(+)small showed little difference from the control cells [2% (±6)] cell death. An increasing trend in the cytotoxicity was observed when PS nanoplastics and proteins formed hard corona complex compared to the values observed when the soft corona formed (Fig. 1 and Table III). The significance of the different trends was confirmed, again, by two-tailed ($p < 0.05$) except for PS(+)large complexes ($p = 0.3$).

The effect of PS nanoplastics and protein corona on A549 cells was studied using flow cytometry (FC). Scatter plots (Fig. 2)

TABLE II. Summary of MTT cytotoxicity assay using A549 cells. The cell viability % is shown for the A549 cells exposed to two concentrations of uncoated PS nanoplastics were used. The results are the average of triplicate, and the error is shown inside the parentheses.

	50 μg ml^{-1}	10 μg ml^{-1}
PS(−)large	60% (25)	82% (10)
PS(−)small	73% (4)	85% (5)
PS(+)large	85% (16)	83% (16)
PS(+)small	80% (5)	81% (5)

TABLE III. Summary of the MTT cytotoxicity assay using A549 cells. The cell viability % is shown for the A549 cells with different nanoplastics exposure conditions. The concentration of PS nanoplastics and proteins were fixed at 50 and 15 μg ml^{-1}, respectively. The results are the average of triplicate, and the error is shown inside the parentheses.

	HSA (−)		LYS (+)	
PS(−)large	95% (5)	Soft corona	89% (7)	Hard corona
PS(−)small	97% (2)		84% (7)	
PS(+)large	87% (8)	Hard corona	89% (4)	Soft corona
PS(+)small	81% (6)		98% (6)	

show the presence of A549 cells, indicated in the major scattering population (80%–90%). Other populations appearing in the low side scattering (SSC) and forward scattering (FSC) intensities are the debris and/or noise. The introduction of PS(−)small, with or without the presence of protein coronae, did not alter the cytogram profiles significantly. The results imply that a majority of the cells are intact, aligning with the cytotoxicity assay results. The same trend can be observed for the PS(−)large complexes with both types of protein coronae (Fig. S1 in the supplementary material).[54] However, for their positively charged analogs, PS(+)small and PS (+)large, another scattering population, in the low FSC, and a

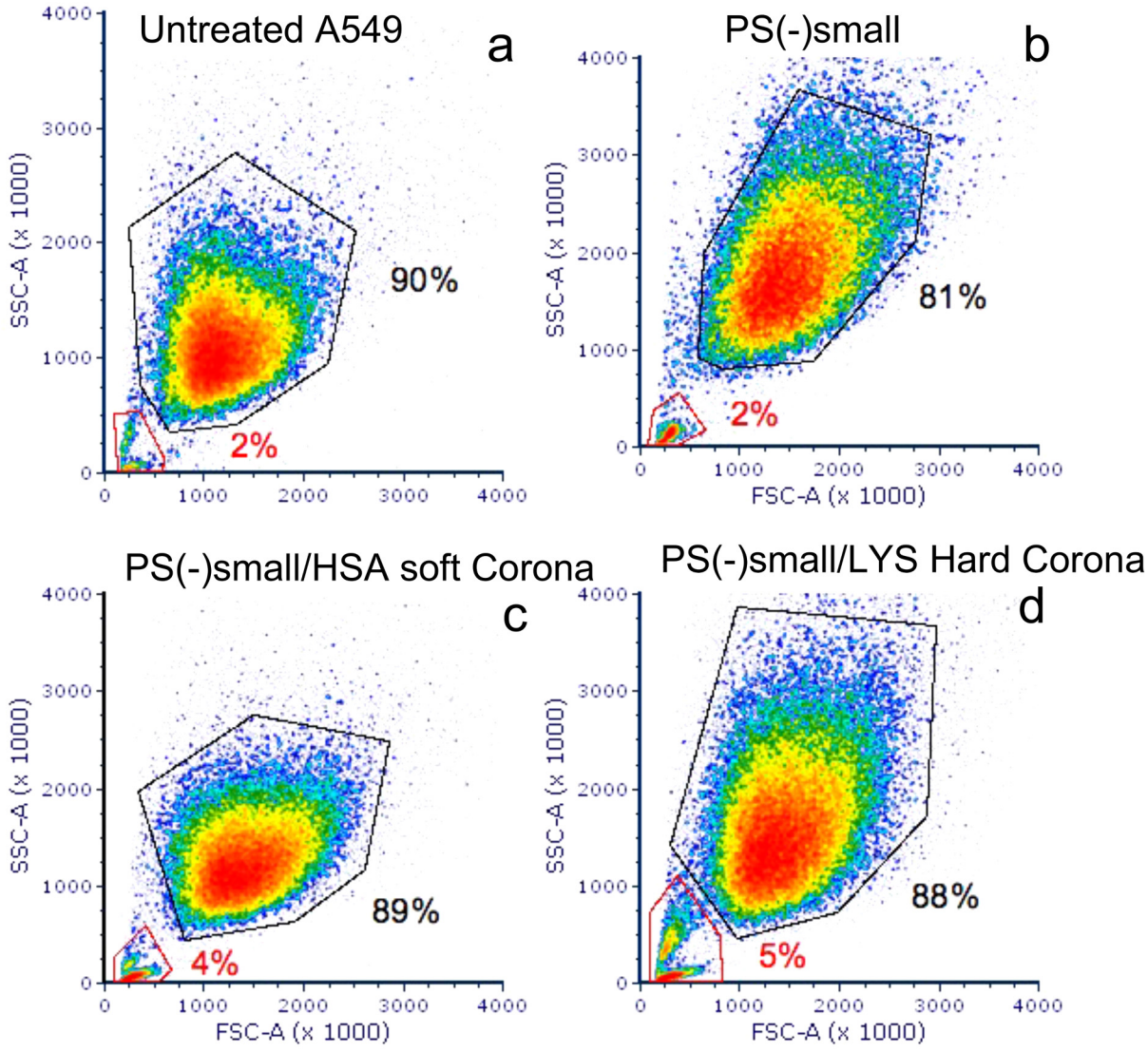

FIG. 2. Cytograms of control A549 cells (a) and those exposed to PS(−) nanoplastics (b), PS(−)/HSA soft corona (c), and PS(−)/LYS hard corona (d). Gating was applied to two identifiable scattering populations.

broad range of SSC intensities appear (Fig. S1 in the supplementary material).[54] Although strong scattering from the PS(+)small and PS(+)large nanoplastics is evident in the control FC experiment, without A549 cells (Fig. S2 in the supplementary material),[54] the additional scattering population appears to have a different SSC (Fig. S2 in the supplementary material).[54] Colloidal aggregation is observed when PS(+)small and PS(+)large nanoplastics are dispersed in DMEM (evidenced in cytograms found in Fig. S1 in the supplementary material),[54] which led to the appearance of the scattering profile.

The FSC and SSC histograms are shown in Fig. 3. The FSC scale increased slightly when PS(−)small (with or without the protein corona) was incubated with the cells, implying little influence on overall cell sizes according to the Mie theory. The relative SSC scale increased in comparison to the control cells, with the bare PS(−)small showing the greatest effect followed by PS(−)small/LYS hard corona complex, and PS(−)small/HSA soft corona complex. The observed trend was also found for PS(−)large complexes (Fig. S3 in the supplementary material).[54] Similarly, for the positively charged particles, the effect of the bare PS nanoplastics appeared to promote the greatest change, and the PS/hard corona complexes either caused greater or a similar extent of change compared to the PS/soft corona complexes. The increase on the SSC scale is related to the cytoplasmic complexity for eukaryotic cells.[32,33] We speculate that the increase in the cellular complexity is attributed to the additional cellular environment present inside the cells and/or internalised PS particles.

The cell uptake process was visualized using fluorescently labeled PS(−)small and A549 cells with nuclei stained with 4′,6-diamidino-2-phenylindole (DAPI) (Fig. 4) by fluorescence microscopy. Prior to and after the staining process, the A549 cells were extensively rinsed, to remove freely floating particles. Under all conditions [except for PS(+)small, which we could not obtain the florescence particles], the cellular uptake of the PS nanoplastics was confirmed (Figs. 5 and 6). The experiment was repeated in the presence of 10% fetal bovine albumin (FBS) to simulate the high concentration of serum albumin (the main component of 10% FBS is bovine serum albumin) in the cells treated with PS(−)small/HSA soft corona (Fig. S4 in the supplementary material).[54] Once more, the PS particles were observed within the cells even in the presence of the 10% FBS. Overall, the penetrated particles appear to surround the nuclei, though it is unclear if the particles are inside the nuclei or not. To verify this, three-dimensional images were created via Z-stacking different focal planes (Fig. 7 and Fig. S5 in the supplementary material).[54] While the particle adhesion on the nuclear membrane is evident visually, no particles were found to be inside the nuclei.

In rare cases, the chromosomes, in the absence of nuclear membrane, are surrounded by PS(−)small though no such case was found for the cells treated with the large nanoplastics. To further investigate this size-dependent effect, the cells were treated with the two size-combination of PS(−) nanoplastics tagged with two distinct fluorescent molecules (image shown in Fig. 7). Indeed, the small PS(−)small particles are shown to interact with the chromosomes more favorably than the PS(−)large. Provided that transmembrane diffusion is an implausible uptake mechanism, the chromosomal interactions likely took place during the prophase or

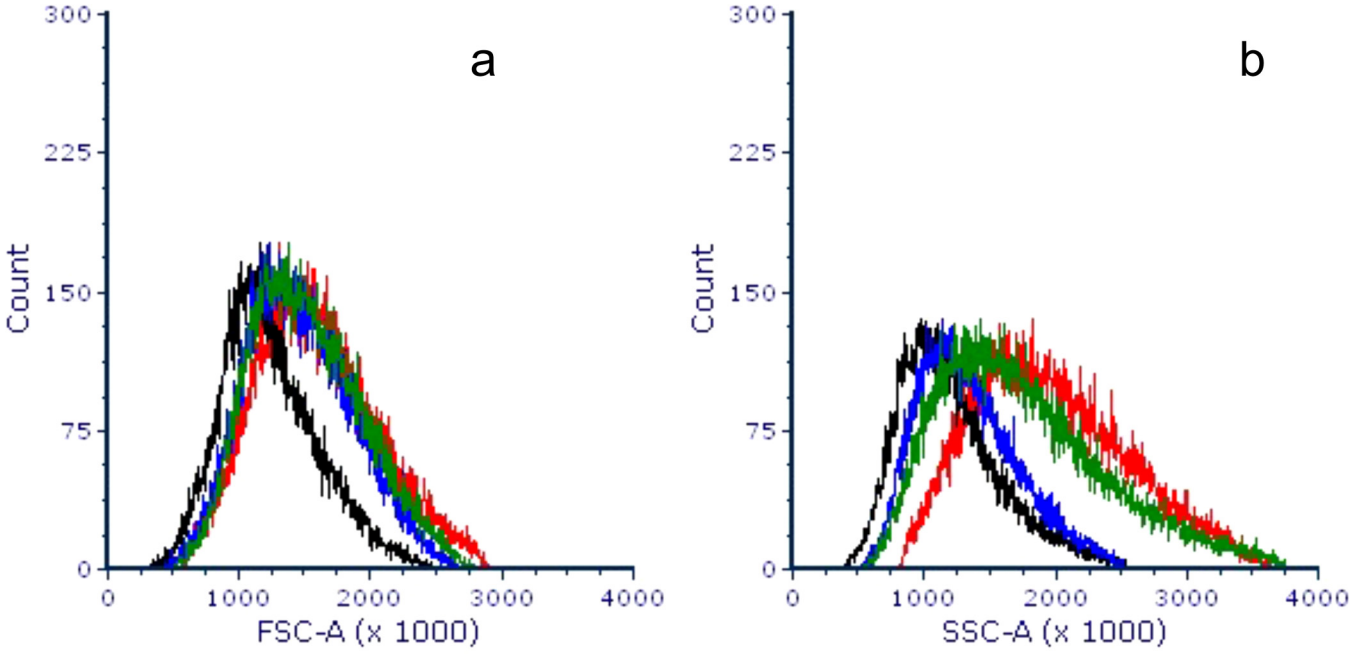

FIG. 3. Forward-scatter (FSC-A) (a) and side-scatter (SSC-A) (b) and histograms of A549 cells (black), exposed to bare PS(−)small nanoplastics (red), PS(−)small/HSA soft corona (blue), and PS(−)small/LYS hard corona (green). Gating was applied to select the cells from major scattering populations shown in Fig. 2.

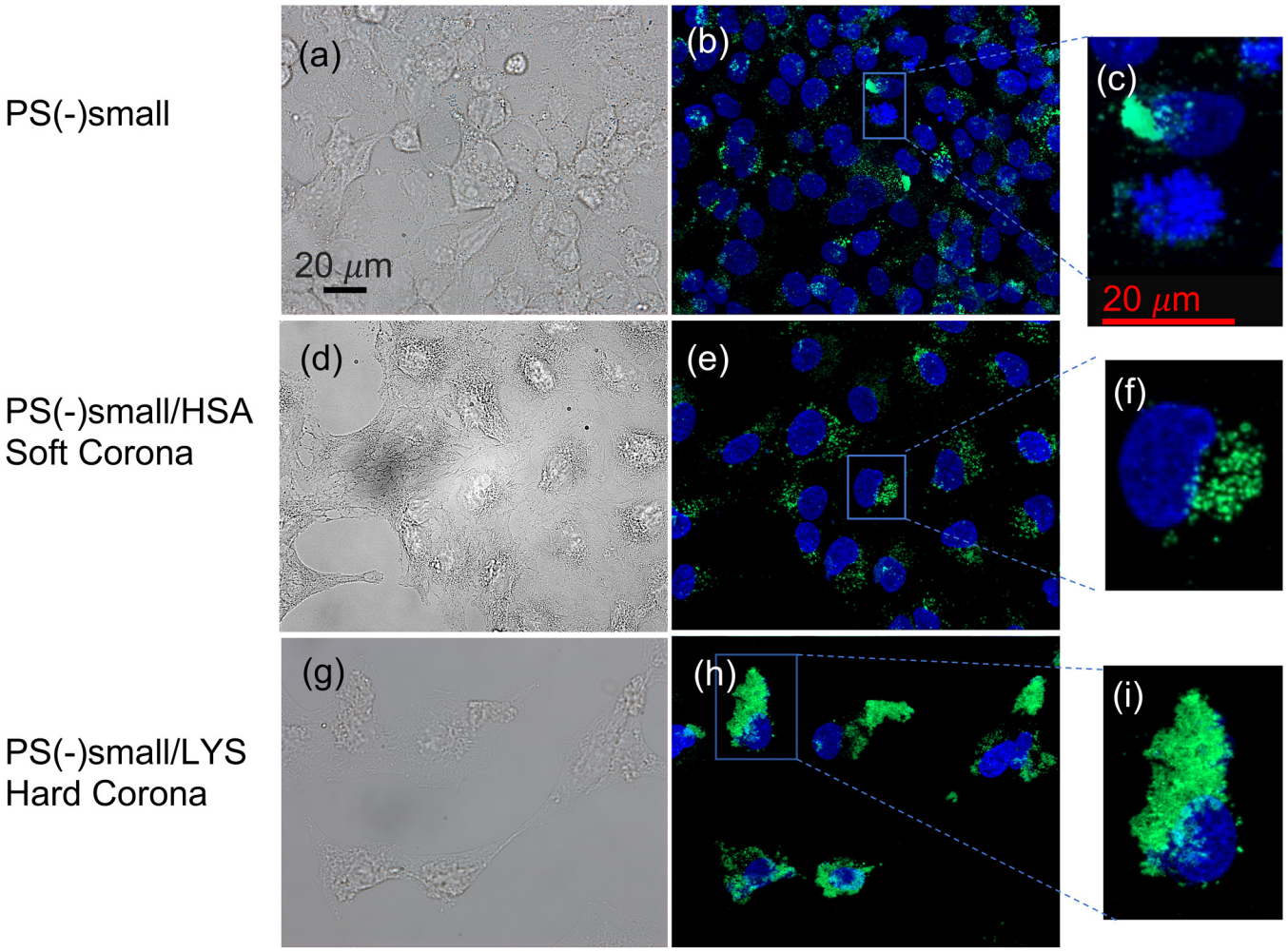

FIG. 4. Bright field (a), (d), and (g) and fluorescence micrographs (b), (e), and (h) of DAPI nuclear stained (blue) A549 cells, treated with fluorescently labeled PS(−)small (green). The enlarged details of the fluorescence micrographs (c), (f), and (i) highlight the individual nuclei with PS nanoplastics. The enlarged image of the cells treated with PS(−)small nanoplastics also features the chromosomes (c).

anaphase mitotic stages, which takes place prior to the nuclear membrane formation.

B. Molecular interactions between cell membrane and PS nanoplastics and PS/protein corona complexes

EIS was used to analyze the effect of PS nanoplastics with and without the presence of soft/hard protein coronae. The EIS spectra were described by an electrical equivalent circuit (EEC) model, shown in Fig. 8(d). The fitting parameters, $R_{membrane}$ and constant phase element (CPE) (shown in Tables IV and V), are used to describe the physical properties of differently treated lipid bilayers. $R_{membrane}$ shows the resistance of the lipid bilayer—how closely packed the bilayers are—to mitigate the ion flows across the membrane. CPEs describe the capacitance and ideality of the capacitor (perfectly homogeneous bilayer when $\alpha = 1.0$).[29,34,35] Additionally, bulk solution resistance ($R_{solution}$) and submembrane capacitance (C_{sub}), describing the Au-tether submembrane reservoir, are used in the model.[34,36] Hereafter, $R_{membrane}$ and CPE values are reported.

Representative EIS Bode plots of lipid bilayers before and after the introduction of bare PSsmall (20 nm), PSsmall with soft protein corona, and hard corona are presented in Figs. 8(a) and 9(a). Regardless of the surface charge, bare PSsmall nanoplastics caused a notable decline in $R_{membrane}$ (as high as a 44% decrease compared to the bare bilayer) was observed with an increasing concentration of the PS nanoplastics. Additionally, a systematic increase in the capacitance values and decreasing α values were observed (fitting summary is found in Tables IV and V). Larger PS nanoplastics, on the contrary, showed insignificant changes to CPE values (Fig. S6 and Table S1 in the supplementary material).[54] $R_{membrane}$ was

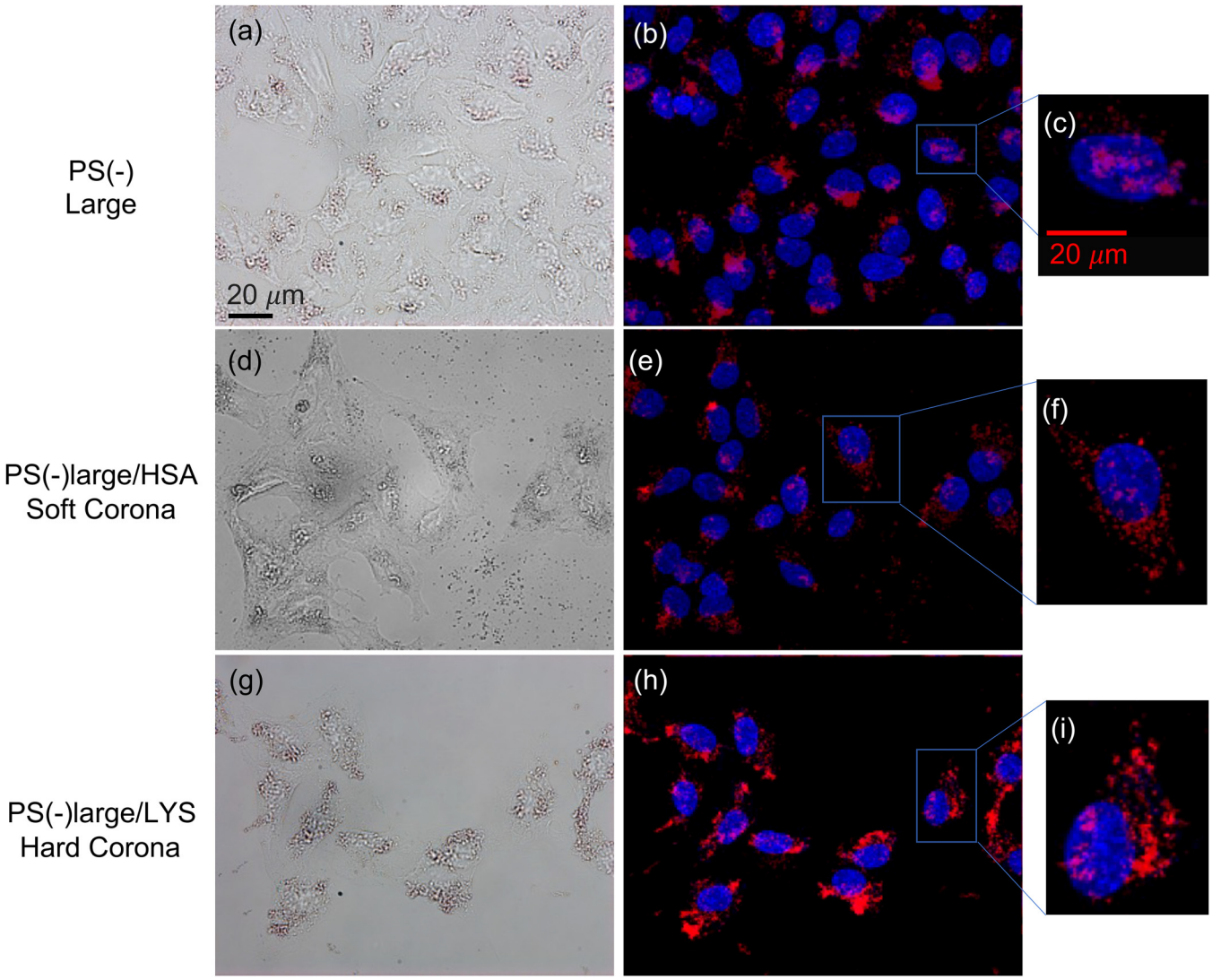

FIG. 5. Bright field (a), (d), and (g) and fluorescence micrographs (b) (e), and (h) of DAPI nuclear stained (blue) A549 cells, treated with fluorescently labeled PS(−)large (red). The enlarged details of the fluorescence micrographs (c), (f), and (i) highlight the individual nuclei with PS(−)large.

observed to increase for both negatively and positively charged particles. These increasing $R_{membrane}$ values are thought to be attributed to the large insulating PS nanoplastics adsorbed on the bilayer surface, inhibiting ion transport across the membrane, without causing significant disruption to the membrane structure.

The effect of free-standing HSA and LYS was also tested prior to assessing the impact of nanoplastics with soft or hard protein corona (Fig. S7 and Table S3 in the supplementary material).[54] After the introduction of both HSA and LYS, marginal changes to the $R_{membrane}$ and CPE values were observed, in some cases, a slight increase. This indicates that both proteins interact with the membrane surface without disturbance to the structural integrity.

Finally, the relevance of the protein corona in nanoplastic-membrane interactions was tested by introducing the PS nanoplastics with either soft or hard protein corona to the bilayer. In these complex systems, the relevance of corona protein was explored by varying the concentration of proteins (50–150 $\mu g\,ml^{-1}$) while the concentration of PS nanoplastics was fixed (250 $\mu g\,ml^{-1}$). The EIS Bode plots of PS(−)small with HSA soft protein corona, at two different HSA concentrations, are presented in Figs. 8(b) and 8(c), and the fitting parameters are summarized in Table V. The disruption of the bilayer was significantly reduced when the concentration of HSA soft corona was 50 $\mu g\,ml^{-1}$ [16% decline in $R_{membrane}$ vs 44% decline with bare PS(−)small]. When the HSA soft corona

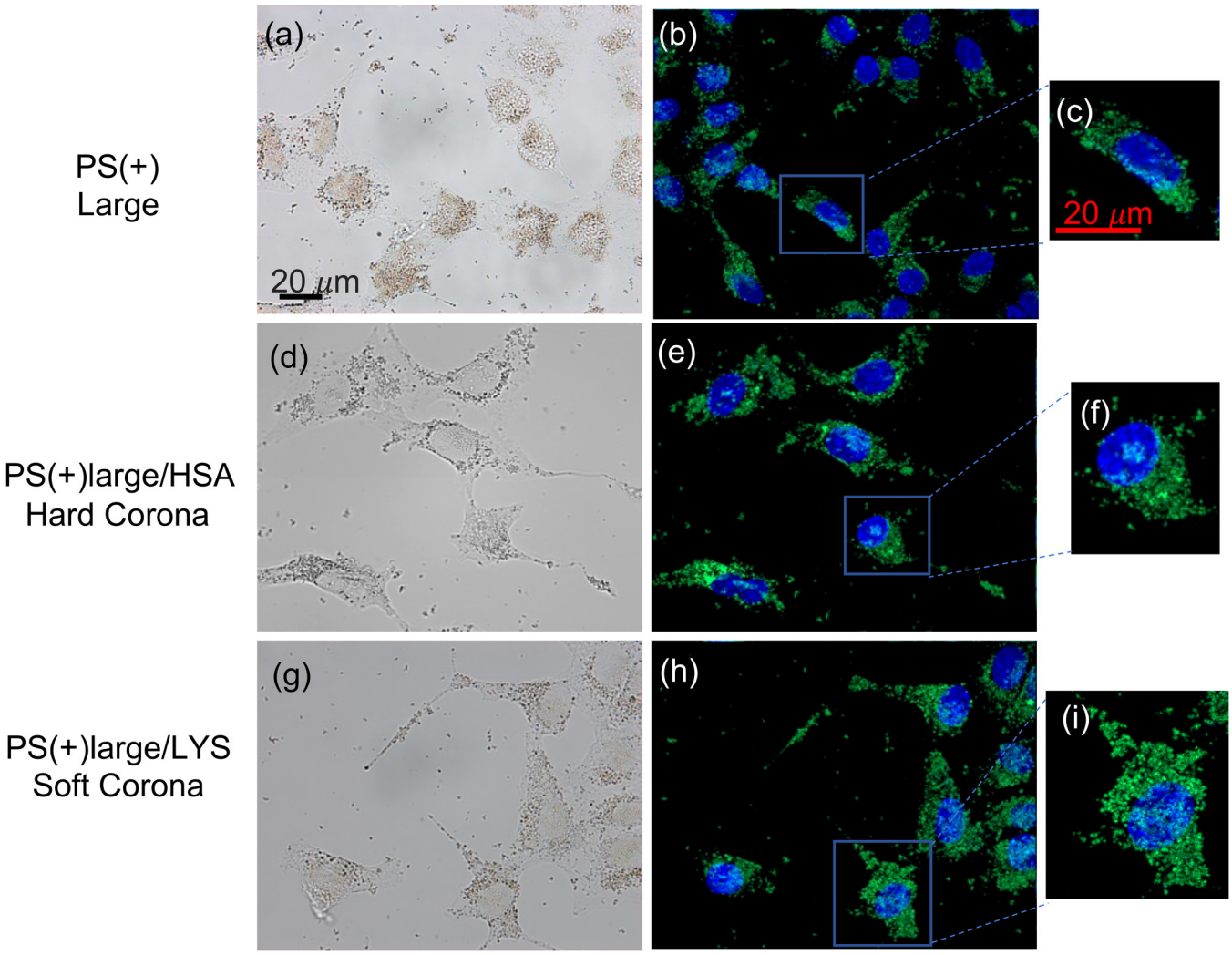

FIG. 6. Bright field (a), (d), and (g) and fluorescence micrographs (b), (e), and (h) of DAPI nuclear stained (blue) A549 cells, treated with fluorescently labeled PS(+)large (green). The enlarged details of the fluorescence micrographs (c), (f), and (i) highlight the individual nuclei with PS nanoplastics.

concentration reached 150 μg ml^{-1}, the $R_{membrane}$ value surpassed that of the control membrane, resembling the behavior of free-standing HSA. For PS(−)small with LYS hard corona, the mitigation effect was found to be minimal, if not, a similar degree of bilayer disruption was observed (40% decline in $R_{membrane}$). Noticeably, when the concentration of hard corona LYS increases from 50 to 150 μg ml^{-1}, the bilayer stability deteriorated further as evidenced by the significant change in $R_{membrane}$ and CPE values while free-standing LYS cause marginal effect (Table V and Table S2 in the supplementary material).[54]

Another set of nanoplastics/hard corona combination [PS(+) small/HSA] was also tested [Fig. 9(b) and Table VI]. Likewise, the membrane stability declined with an increasing concentration of hard corona participating HSA, as seen by the decreasing $R_{membrane}$ and CPE values. Intriguingly, LYS soft protein corona around PS(+)small did not mitigate the membrane disruption (Fig. 9 and Table VI), instead, it amplified the destabilization effect with increasing LYS concentration (e.g., the $R_{membrane}$ % change increased from −46% to −63% with respect to the control bilayer when the LYS concentration increased from 50 to 150 μg ml^{-1}). This shows that the membrane stability (or reduction of disruption caused by bare PS nanoplastics) is not simply dependent on the type of corona formed but a combination of corona and protein types.

The extent of membrane structural alteration caused by the PS nanoplastics and the nanoplastic/protein corona complexes was studied using NR. The seven slab layers were used to accommodate the NR profiles of the tethered lipid bilayer, namely, Si, SiOx, Cr

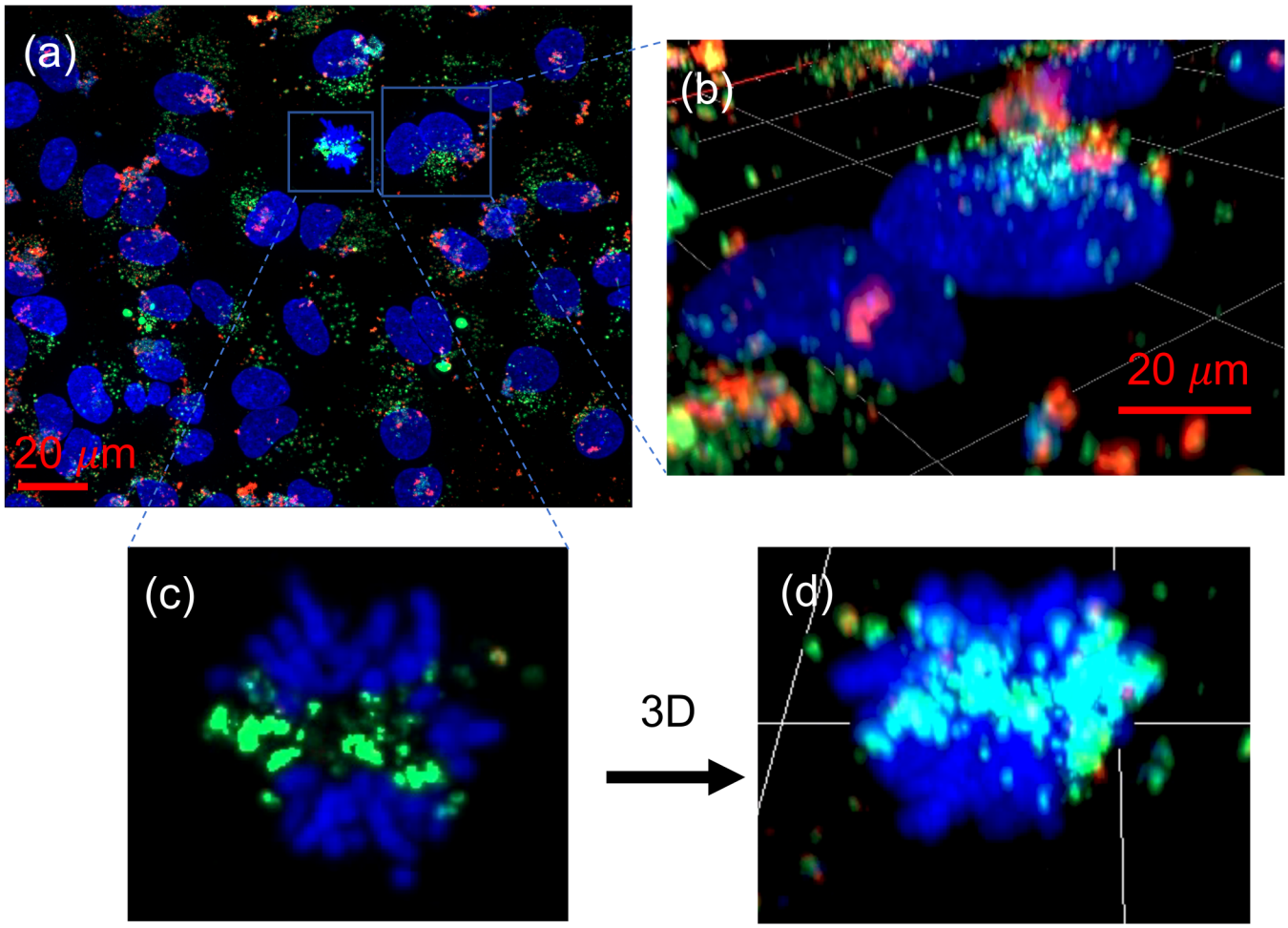

FIG. 7. Fluorescence micrographs (a) of DAPI nuclear stained (blue) of A549 cells treated with the combination of fluorescently labeled PS(−)small (green) and PS(−) large (red). An enlarged image (b) and the three-dimensionally reconstructed images (c) and (d) and individual nuclei (c) and chromosomes (b) and (d).

(CrOx), Au, tether, hydrophobic chains, and POPC headgroup. The inorganic layers and the tether regions were fixed to the values fitted for the control samples, while the hydrophobic chains and POPC headgroups were fitted. Hydrophobic chains of DPhyTL and POPC merged in this fitting model. The lack of neutron scattering length density (nSLD) contrast between the hydrophobic moieties of these two lipid molecules did not justify the presence of two independent slabs. The nSLD of the hydrophobic chains were fixed to -0.5×10^{-6} Å^{-2}. Herein, we report the change in the thickness, nSLD, and solvent vol. % of the hydrophobic chains and POPC headgroup before and after the introduction of PS nanoplastics in the presence or absence of the protein corona.

The PSsmall, regardless of their surface charges, increased solvent penetration on the POPC headgroup by approximately 20% and lowered the nSLD from $\sim 2.0 \times 10^{-6}$ to $\sim 1.5 \times 10^{-6}$ Å^{-2} (NR and SLD profiles are shown in Fig. 10 and Fig. S8 in the supplementary material,[54] and fitting parameters are shown in Tables VII and VIII). Furthermore, the tightly packed hydrophobic chains were found to be occupied by the solvent when bare PS(−)small nanoplastics were introduced [0%(0.1) for control vs 2%(0.1)]. The size effect was also investigated using PS(−)large (Fig. S9 in the supplementary material).[54] Addition caused insignificant changes (Table S3 in the supplementary material)[54] to the structural properties of the bilayer, which agrees with the EIS measurements. The effects of proteins on the POPC tethered bilayer were independently assessed. A notable effect was seen in the thinning of the hydrophobic chains [3.0 Å (±0.1)], and the decrease in the solvent penetration in the POPC headgroup [by 29% (±2)]. For LYS (Fig. S10 in the supplementary material),[54] thinning on the hydrophobic chains was observed while the POPC headgroup appeared to experience a thickening effect [by 2.4 Å (±0.2)] (Table S4 in the supplementary material).[54] The nSLD of the POPC headgroup increased by $\sim 0.5 \times 10^{-6}$ Å^{-2}. Finally, a weakly increasing trend in the solvent penetration in the POPC headgroup could be observed [increase in ~6% (±2)].

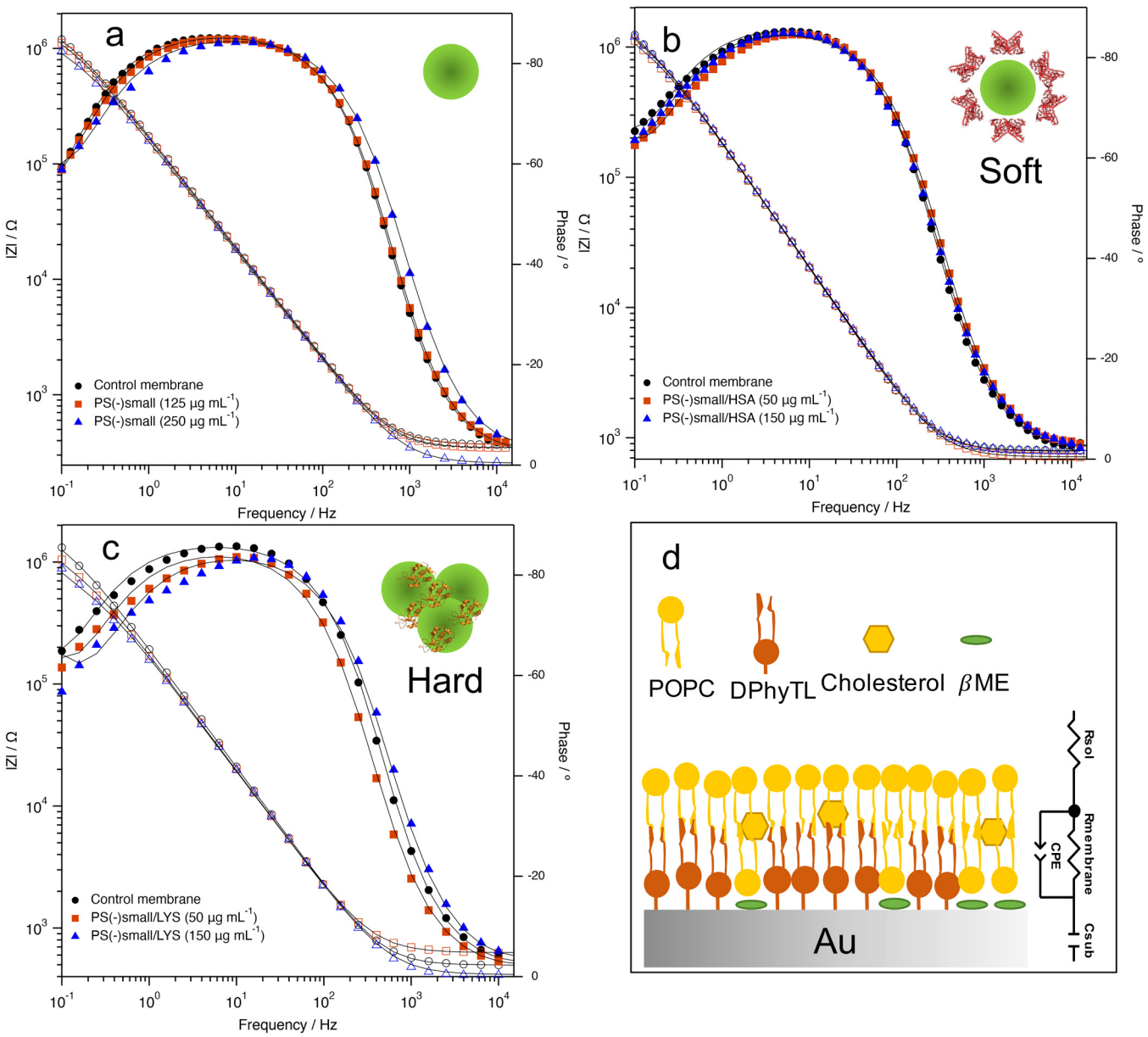

FIG. 8. Representative EIS Bode plots (filled marker shows phase shift and open symbol shows impedance) of POPC tethered bilayer (labeled "control membrane"), bilayer exposed to PS(−)small nanoplastics at different concentrations (a); bilayer exposed to PS(−)small/HSA soft corona complexes at different HSA concentrations (b); and bilayer exposed to PS(−)small/LYS hard corona at different LYS concentrations (c). The schematics (d) depict the POPC tethered bilayer with different components and the EEC model used to fit the Bode plots.

When PS(−)small combined with the HSA soft corona, the change in the solvent penetration in both the hydrophobic chains [0%(±0.1) for control vs 0%(±0.1) with PS(−)small/HSA soft corona] and the POPC headgroup became insignificant [50%(±2) for control vs 53%(±3) for PS(−)small/HSA soft corona]. A decline in the nSLD of the POPC headgroup was also observed, the extent of which may be comparable to the effect of the bare PS(−)small nanoplastics [1.61×10^{-6} Å^{-2} (±0.10)]. Furthermore, PS(−)small/HSA soft corona appears to thin the POPC headgroup by ∼1.0 Å (±0.2)—such an effect is also seen when bilayer interacts with HSA alone (Fig. S10 and Table S5 in the supplementary material).[54] PS(−)small/LYS hard corona caused a significant thinning effect on the POPC headgroup

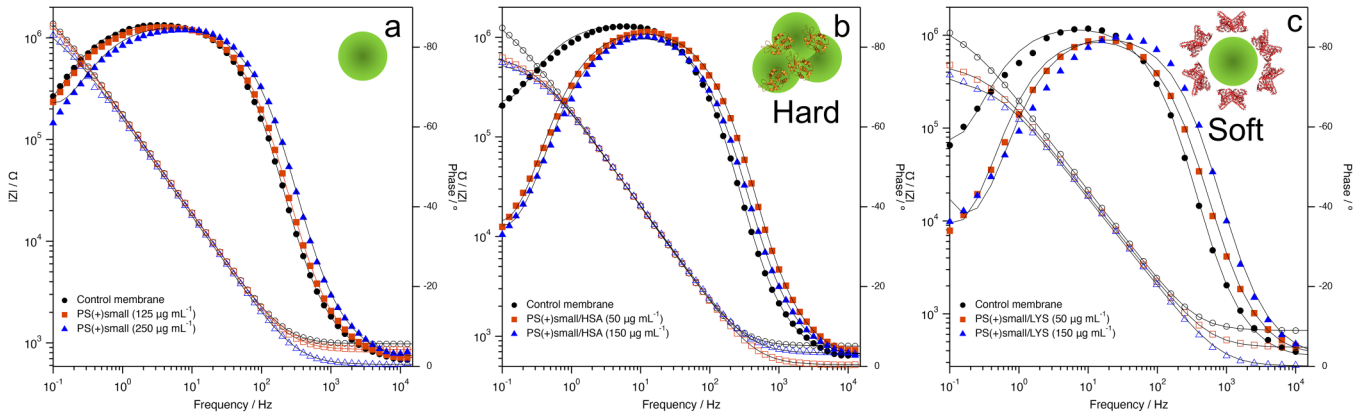

FIG. 9. Representative EIS Bode plots (filled marker shows phase shift and open symbol shows impedance) of POPC tethered bilayer (labeled "control membrane"), bilayer exposed to PS(+)small nanoplastics at different concentrations (a); bilayer exposed to PS(+)small/HSA hard corona complexes at different HSA concentrations (b); and bilayer exposed to PS(+)small/LYS soft corona at different LYS concentrations (c).

TABLE IV. EIS fitting parameters for tethered lipid bilayers before and after the introduction of PS nanoplastics, at different concentrations. Uncertainties are reported in parentheses. The change in the fitting parameters with respect to the control data (bare lipid bilayers) is shown as a percentage.

Fitting parameters	Control	PS(−)small 125 μg ml^{-1}	PS(−)small 250 μg ml^{-1}	Control	PS(+)small 125 μg ml^{-1}	PS(+)small 250 μg ml^{-1}
$R_{membrane}$/MΩ cm^2	1.26 (0.03)	1.06 (0.02)/−16%	0.70 (0.03)/−44%	1.30 (0.05)	1.21 (0.04)/−7.1%	0.87 (0.01)/−33%
CPE/μF cm^{-2} s$^{(1-\alpha)}$	1.29 (0.02)	1.38 (0.01)/+7.0%	1.57 (0.04)/+22%	1.51 (0.07)	1.52 (0.01)/+0.4%	1.60 (0.04)/+6.0%
α	0.954 (0.006)	0.950 (0.006)/−0.4%	0.939 (0.01)/−1.5%	0.958 (0.001)	0.953 (0.01)/−0.5%	0.949 (0.01)/−0.9%

TABLE V. EIS fitting parameters for tethered lipid bilayers before and after the introduction of PS(−)/protein corona complexes at different protein concentrations, with a fixed concentration of PS(−)small nanoplastics of 250 μg ml^{-1}. Uncertainties are reported in parentheses. The change in the fitting parameters with respect to the control data (bare lipid bilayers) are shown as a percentage.

Fitting parameters	Control	Soft corona PS(−) small/HSA 50 μg ml^{-1}	PS(−)small/HSA 150 μg ml^{-1}	Control	Hard corona PS(−) small/LYS 50 μg ml^{-1}	PS(−)small/LYS 150 μg ml^{-1}
$R_{membrane}$/MΩ cm^2	0.75 (0.02)	0.68 (0.02)/−9.3%	0.81 (0.02)/+8.0%	0.91 (0.05)	0.63 (0.04)/−31%	0.55 (0.04)/−40%
CPE/μF cm^{-2} s$^{(1-\alpha)}$	1.51 (0.05)	1.46 (0.02)/+3.3%	1.44 (0.02)/−0.7%	1.43 (0.03)	1.56 (0.03)/+9.0%	1.54 (0.05)/+7.7%
α	0.955 (0.02)	0.947 (0.02)/−0.8%	0.946 (0.01)/−1.3%	0.953 (0.002)	0.936 (0.001)/−1.8%	0.925 (0.005)/−2.9%

TABLE VI. EIS fitting parameters for tethered lipid bilayers before and after the introduction of PS(+)small/protein corona complexes at different protein concentrations, with a fixed concentration of PS(+)small nanoplastics of 250 μg ml^{-1}. Uncertainties are reported in parentheses. The change in the fitting parameters with respect to the control data (bare lipid bilayers) are shown as a percentage.

Fitting parameters	Control	Hard corona PS(+)/ HSA 50 μg ml^{-1}	PS(+)/HSA 150 μg ml^{-1}	Control	Soft corona PS(+)/ LYS 50 μg ml^{-1}	PS(+)/LYS 150 μg ml^{-1}
$R_{membrane}$/MΩ cm^2	0.87 (0.02)	0.54 (0.02)/−38%	0.48 (0.01)/−45%	0.70 (0.03)	0.38 (0.10)/−46%	0.26 (0.09)/−63%
CPE/μF cm^{-2} s$^{(1-\alpha)}$	1.11 (0.02)	1.04 (0.06)/+6.4%	1.04 (0.07)/+6.4%	1.22 (0.02)	1.19 (0.02)/−2.5%	1.28 (0.03)/+0.5%
α	0.970 (0.001)	0.957 (0.001)/−1.3%	0.951(0.001)/−2.0%	0.954 (0.002)	0.937 (0.003)/−1.8%	0.940 (0.005)/−1.5%

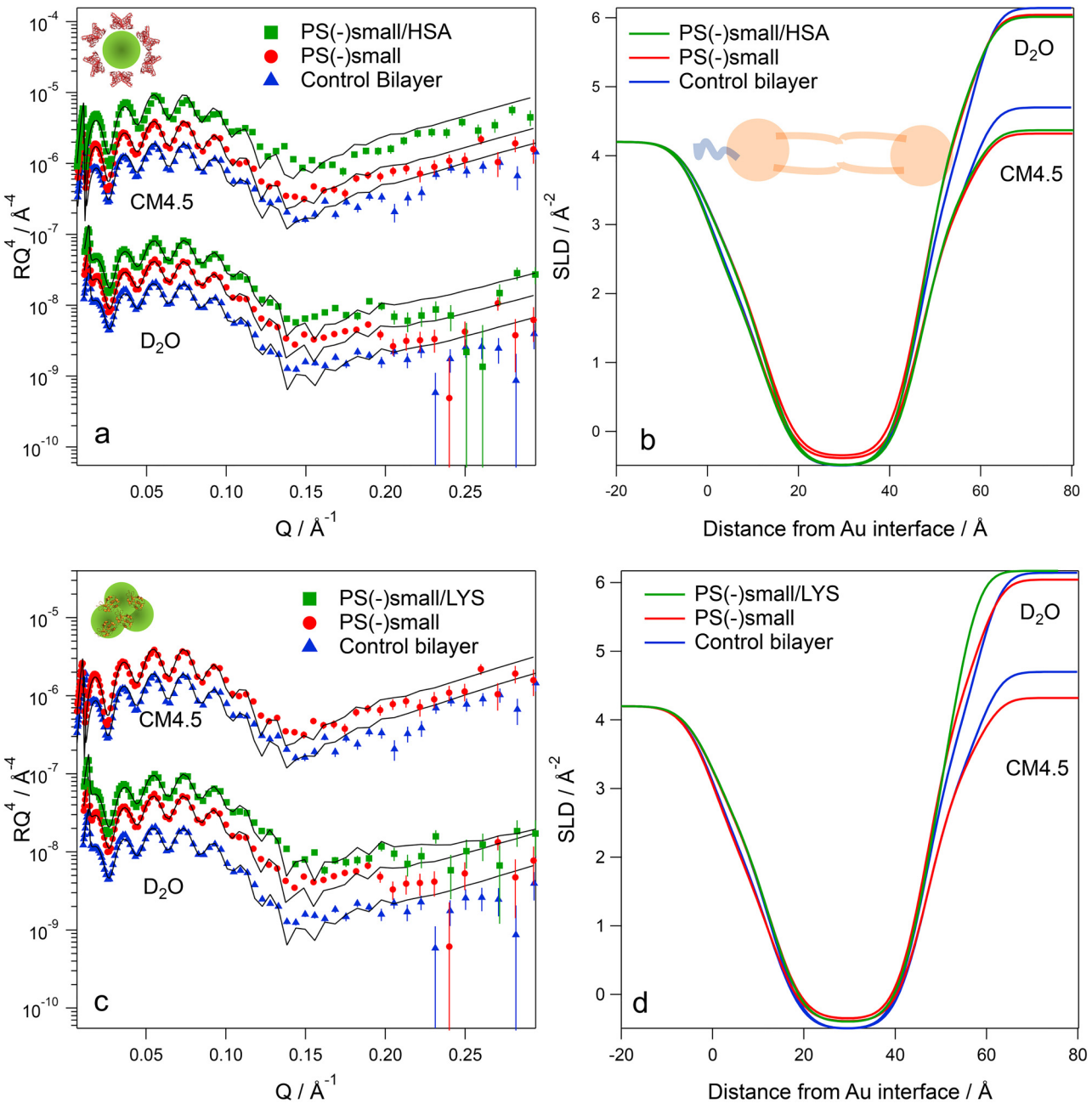

FIG. 10. NR (RQ4 vs Q) profiles of POPC/cholesterol tethered bilayers, with and without the PS(−)small/protein corona complexes (a) and (c). The corresponding nSLD profiles are presented (b) and (d), highlighting the structural change in the tethered bilayer (tether, hydrophobic chains, POPC headgroup, and bulk solvent regions are shown).

[~4.5 Å(±0.5)], and a greater amount of the aqueous solvent penetration in the headgroup was observed [+7%(±2) compared to the control], although not as great as that caused by bare PS(−)small [+17%(±2)]. Here, a similar extent of disruption in the hydrophobic chains could be observed for bilayers with PS(−)small/LYS hard corona complexes to the bilayer with bare PS(−)small [2%(±0.1)].

The reflectivity profiles of POPC tethered bilayers with PS(+) small and protein coronae were also collected. When HSA formed

TABLE VII. Summary of NR fitting parameters for POPC tethered lipid bilayer with and without PS(−)small or PS(−)small/protein corona complexes. The concentration of the PS nanoplastics was fixed at 250 μg ml^{-1} and at 150 μg ml^{-1} for the proteins.

	Control bilayer	PS(−)small	PS(−)small/HSA soft corona	PS(−)small/LYS hard corona
Thickness/Å				
Hydrophobic chains	34.0 (0.1)	34.3 (0.3)	33.1 (0.2)	34.3 (0.1)
POPC headgroup	12.0 (0.4)	11.9 (0.4)	12.0 (0.3)	7.5 (0.5)
nSLD/10^{-6} Å^{-2}				
Hydrophobic chains	−0.5 (fixed)	−0.5 (fixed)	−0.5 (fixed)	−0.5 (fixed)
POPC headgroup	1.98 (0.02)	1.53 (0.04)	1.61 (0.10)	1.52 (0.02)
Solvent vol. %				
Hydrophobic chains	0.0 (0.1)	2.0 (0.1)	0.0 (0.1)	2.0 (0.3)
POPC headgroup	50 (2)	67 (2)	53 (2)	57 (2)

a hard corona with PS(+)small, the complex caused a notable thickening effect in the hydrophobic chains [+4.2 Å (±0.2)]. A structural change in the headgroup was observed, along with greater solvent penetration [28% (±2)] and a decrease in the nSLD [from 1.92×10^{-6} (±0.09) to 1.53×10^{-6} (±0.03) Å^{-2}]. The addition of PS(+)small/LYS soft corona complex provided a similar structural change to PS(+)small, except that the decrease in the nSLD of the headgroup was not as pronounced.

III. DISCUSSION

The present study compares the cellular interactions of PS nanoplastics (of different sizes and charges) with HSA and LYS participating as soft or hard protein corona at two different complexities, namely, *in vitro* cells and model lipid bilayers. In an attempt to relate the findings from these systems, a summary of each experiment, conducted in this study, is presented in Table IX.

A. The surface charge and size effect: Membrane disruption, cytotoxicity, and chromosomal interaction

Mild cytotoxicity was observed in the cells with the bare PS particles. There was no clear correlation between cell death and the physical properties of PS nanoplastics (size and surface charge) in this study. Although there was no clear size dependency observed in the cytotoxicity, a clear size trend is found in the experiments involving a model bilayer. Membrane disruption was observed for PSsmall (20 nm), while PSlarge (200 nm) did not promote any measurable disruption to the POPC tethered bilayer. Based on these observations, one could expect particles within a size threshold to cause bilayer disruption, though identifying the threshold was outside the scope of this study. Combined results from A549 cells and a model bilayer indicate that the level of membrane disruption by these nanoplastics has little influence on cytotoxicity. Nevertheless, there remains a possibility that nanoplastics are indirectly responsible membrane disruption. As highlighted elsewhere,[14,37–39] nanoplastics in cellular environments and *in vivo* settings are linked to enhancing oxidative stress. Excess reactive oxygen species have previously been demonstrated to cause lipid oxidation, resulting in significant alteration to membrane structure.[36]

In rare cases, PSsmall were found in the vicinity of chromosomes with no nuclear membrane around; however, this was not observed for PSlarge (Fig. 7 and Fig. S5 in the supplementary material).[54] This suggests that PS nanoplastics of a smaller size (20 nm) are able to interact with chromosomes prior to nuclear membrane formation, during the cell mitosis—likely prophase-anaphase. The observed phenomenon is only qualitatively observed, and if at all, the mechanistic process remains speculative. However, recent studies[19,40] also have shown chromosol interactions and aberrations caused by PS nanoplastics (100 nm and smaller), supporting that this phenomenon is not unique to the nanoplastic and cell types

TABLE VIII. Summary of NR fitting parameters for POPC tethered lipid bilayer with and without PS(+)small or PS(+)small/protein corona complexes. The concentration of the PS nanoplastics was fixed at 250 μg ml^{-1} and at 0.15 μg ml^{-1} for the proteins.

	Control bilayer	PS(+)small	PS(+)small/HSA hard corona	PS(+)small/LYS soft corona
Thickness/Å				
Hydrophobic chains	30.2 (0.2)	30.7 (0.2)	34.4 (0.2)	30.3 (0.4)
POPC headgroup	11.9 (0.1)	11.9 (0.4)	12.0 (0.6)	11.9 (0.1)
nSLD/10^{-6} Å^{-2}				
Hydrophobic chains	−0.5 (fixed)	−0.5 (fixed)	−0.5 (fixed)	−0.5 (fixed)
POPC headgroup	1.92 (0.09)	1.52 (0.02)	1.53 (0.03)	1.76 (0.04)
Solvent vol. %				
Hydrophobic chains	10 (1)	4 (2)	11 (1)	11 (1)
POPC headgroup	59 (1)	78 (2)	87 (2)	76 (3)

TABLE IX. Comparative findings of *in vitro* and model POPC tethered lipid bilayer experiments.

	In vitro A549 cells		POPC/cholesterol tethered lipid bilayer
Cytotoxicity assay	1. Effects due to particle size and charge were not observed. 2. Protein corona mitigated the cytotoxicity in most cases. PS nanoplastics with hard protein corona imparted more significant cytotoxicity than with soft corona.	EIS/NR	1. Effect due to particle size was observed, while charge effect was not observed. 2. Protein corona mitigated the bilayer disruption in most cases. Generally, the hard corona led to more severe bilayer disruption. However, when LYS participated in soft corona formation, it did not mitigate the disruptive effect. 3. The observation of membrane damage was limited to the POPC headgroup—the hydrophobic chains were largely unaffected.
Flow cytometry and fluorescence microscopy	1. The granularity of the cells increased when PS nanoplastics were added (with or without the protein corona). 2. Cell uptake is implied in flow cytometry and observed in fluorescence images. 3. The PS particles were inside the cells and adhered to the nuclear membrane—none or few particles were inside the nuclei.		

used in this work. This observation is particularly intriguing because of the potential link between nanoplastics with delayed reproduction[15–17] and transgenerational effects,[17] opening the possibility of PS nanoplastics sized <100 nm interacting with DNA.

B. The effect of soft and hard protein coronae

There is no ambiguity that HSA and LYS protein coronae, whether soft or hard, altered the way PS nanoplastics interacted with both *in vitro* cells and the POPC tethered bilayer. In most cases, the presence of the protein corona mitigated the impact of PS nanoplastics on the bilayer disruption and the extent of cytotoxicity. Of the two types of protein coronae, the soft corona showed a greater extent of mitigation on the cytotoxicity than the hard corona. This observed trend was independent of the type of protein (HSA or LYS) participating in the soft or hard corona and the PS particle size. This difference may be correlated with the aggregated fractal-like morphology of hard corona, which is known to promote cellular uptake[41] and cytotoxicity for some cell types.[42] Notably, we demonstrated the effect of protein corona at a very low concentration (20 μg ml^{-1}) where a typical protein concentration used for *in vitro* experiments is tenfold to 100-fold higher.[24,25] The result emphasizes the importance of understanding the biointerface properties of nanoplastics/nanoparticles in assessing their biological outcome.

Likewise, the PS/HSA soft corona complex exhibited a greater extent of mitigation in terms of the nonspecific disruption of the lipid bilayer (of the model membrane), when compared with the PS/HSA hard corona complex. However, for LYS, regardless of the nature of the protein corona formed, the mitigation effect was limited. The effect of the protein corona on a bilayer has been documented for other kinds of nanoparticles[26,43–45] and some nanoplastics.[19,25,45] Di Silvio *et al.*[46] reported that PS nanoplastics with a hard protein corona (proteins recovered from serum) did not promote apparent damage to a supported DOPC lipid bilayer. Intriguingly, when a soft corona was present with the hard corona, the DOPC bilayer experienced more severe disruption. The authors highlighted that the proteins participating in soft corona formation affected the lipid membrane differently than the free-standing proteins. The report aligns with our findings of the LYS soft corona, while the HSA soft corona preserved its behavior. The difference between HSA and LYS in soft protein corona emphasizes that the role of proteins within the corona around PS nanoplastics should be discussed on a case-by-case basis.

In some reports,[24,25] the cell internalization of nanoparticles was strongly inhibited by the presence of protein corona. However, this was not the case for the PS nanoplastics precoated with HSA and LYS protein corona, where a cell internalization was still observed. Fleischer *et al.*[25] suggest that different cellular responses occur depending on whether the secondary structure of corona proteins is preserved.

C. Implications to cellular uptake mechanisms

Under all the conditions tested in this work, we observed cellular uptake of PS nanoplastics and PS/protein corona complexes. Two likely uptake mechanisms are transmembrane diffusion[47] and endocytosis,[48] previously suggested for nanoparticle uptake. In order for transmembrane diffusion to occur, severe disruption in the lipid bilayer is necessary, especially, for the nanoplastic sizes tested in this work. However, the extent of disruption was limited to the hydrophilic headgroup of POPC. For this reason, the possibility of transmembrane diffusion can be excluded. Furthermore, the EIS experiment demonstrated the adhesion of all PS nanoplastics (and PS/protein corona complexes) onto the lipid bilayer, where cell adhesion is known to be a crucial step for endocytosis.[24,49]

IV. CONCLUSION

Numerous reports have investigated the adverse effects caused by nanoplastics using model organisms and *in vitro* cell lines. Few have attempted to deconvolute the factors contributing toward the biological outcomes. The importance of protein corona in the subsequent biological effects of nanoparticles has been highlighted strongly by many authors in the literature. The biological role of protein corona has also varied from nanoparticle to nanoparticle, as well as based on the cell types used. Due to the complex nature of protein corona found *in vivo* and *in vitro*, separating the effects

of soft and hard protein corona has been challenging. Here, we used a model with soft and hard protein corona around PS nanoplastics to assess their biological outcome.

The introduction of bare PS nanoplastics (20 and 200 nm) to the A549 cells in serum-free media caused mild cytotoxicity. There was no clear correlation between cell death and the physical properties of PS nanoplastics (size and surface charge) in this study. The bilayer damage observed in the POPC tethered bilayer, however, was PS particle size-dependent—the large particles (200 nm) did not induce any membrane disruption. However, there may be a size threshold (between 20 and 200 nm) for PS nanoplastics to be able to disrupt bilayer.

The PS nanoplastic interaction with cells was not limited to membrane adhesion, and particle uptake was implied with the FC and confirmed with fluorescence microscopy. By qualitatively assessing the images of the fluorescently tagged PS nanoplastics and nuclei stained A549 cells, many of the particles were observed inside the cells and some were found to be localized around the nuclei. The three-dimensionally reconstructed images showed the absence of particle penetration into the nuclei, although they appeared to be adhering to the nuclear membrane surface.

Whether soft or hard, the presence of protein corona mitigated the cytotoxic actions by the PS nanoplastics. When comparing the different types of the protein corona, PS nanoplastics with a hard corona showed more severe cytotoxicity. This observation did not depend on the type of protein used (HSA and LYS) or the size of the PS particles. In all cases, an increase in the cell granularity was observed via an FC experiment, which may be attributed to the particle uptake and/or the additional cellular environment created inside the cells. Visually, we could confirm the particle cell uptake, regardless of the types of protein corona.

There was also an indication that chromosomes were found close to PSsmall. However, when the cells were incubated with PSlarge, chromosomes were not observed. To further assess this phenomenon, both small and large PS(−) particles were incubated with A549 cells for 24 h. The chromosomes were, indeed, captured in fluorescence images, and predominantly, the smaller PS particles were observed close to the chromosomes. Given that PS nanoplastics have been associated with reports on delayed reproduction[15–17] and transgenerational effects,[17] such an observation at a cellular level is intriguing and demonstrates the possibility that small PS nanoplastics (20 nm) interact with DNA. Although the exact mechanism behind the pathway to localize with chromosomes remains questionable, we hypothesize that the PS particles may have interacted with the chromosomes during the cell splitting stage. The PS particles alone are unable to penetrate the nuclear membrane. To surpass this physical barrier, PS particles must interact with the chromosomes when the membrane property is dynamically altering—likely during the prophase and anaphase mitotic processes.

Overall, we demonstrated that the biological outcomes of PS nanoplastics are dependent on the nature of the protein corona and the intrinsic properties of the nanoplastics. It is imperative to have prior knowledge about the protein corona and the molecular details of the cellular membrane, in order to link the nanoplastic property and the *in vitro* biological outcome. The current study has addressed short-term exposure to nanoplastics, while nanoplastic exposure is expected to be in the long-term.

V. METHODS AND MATERIALS

A. Materials

For *in vitro* experiments, the following reagents were used without further purification: 3-[4,5-dimethylthiazole-2-yl]-2,5-diphenyltetrazolium bromide (MTT) (abcam, ab322092 MTT cell proliferation kit), DAPI (D1306, Thermo Fischer Scientific), Dulbecco's modified Eagles's medium (11885092, DMEM, low glucose, pyruvate, Gibco®, Life Technologies New Zealand), fetal bovine serum (FBS) (10091148, FBS, qualified, New Zealand, Life Technologies New Zealand), Gibco® antibiotic-antimycotic, 1% trypsin/EDTA (Life Technologies New Zealand), and Dulbecco's PBS (DPBS). The A549 cells were generously donated by Professor John Taylor, University of Auckland, New Zealand (originally from ATCC).

Likewise, the following reagents were used without further purification, unless otherwise specified: ultrapure water (resistivity = 18.2 MΩ, Milli Q, Merck Millipore), ethanol (analytical grade, ECP), POPC (Avanti), cholesterol (>99%, Avanti), carboxylic-terminated PS nanoplastics [PS(−)], and amidine-terminated PS nanoplastics [PS(+)] were purchased from Sigma-Aldrich (CML Latex beads, 0.02 μm and amidine latex beads, 0.02 μm, Thermo Fisher Scientific). Larger PS nanoplastics functionalized with amidine groups [PS(+) large] were also purchased from Thermo Fisher Scientific (Amidine Latex beads 0.02 μm). Larger PS nanoplastics functionalized with carboxylic acid [PS(−) large] were synthesized via an emulsion-free polymerization method described elsewhere.[50] Lyophilized HSA (albumin from human serum, essentially fatty acid free) and LYS (from hen egg white) were sourced from Merck. For the fluorescence microscopy experiments, all of the fluorescently tagged PS nanoplastics were purchased from ThermoFisher Scientific New Zealand (carboxylate-modified microspheres, 0.02 μm, yellow-green fluorescent, FluoSpheres™ amine-modified microspheres, 0.2 μm, yellow-green fluorescent, FluoSpheres™, carboxylate-modified microspheres, 0.2 μm, orange-fluorescent). For model membrane studies, tris (Merck) buffer with 10 mM NaOH (99.5%, ECP) was used. PS nanoplastics were extensively dialyzed against ultrapure water, prior to conducting any further characterization. For neutron reflectometry experiments, D_2O was provided by the Australian Nuclear Science and Technology Organisation (ANSTO).

B. Cytotoxicity assay

A549 cells were cultured in T-75 flasks, at 37 °C in 5% CO_2, in DMEM, supplemented with 5% FBS and 1% Gibco® antibiotic-antimycotic. In a 96-well plate, 3000 cells were cultivated, and when 70–80% confluency was achieved, each well was rinsed with PBS solution to remove proteins present in the FBS solution. Finally, the desired concentrations of PS nanoplastics or PS/protein corona complexes (dispersed in DMEM without FBS) were added, allowing 18 h of incubation time prior to the MTT assay. Cell viability% was determined with triplicates according to the formula

$$\text{Cell viability\%} = \frac{\text{abs}_{\text{sample}}\text{-abs}_{\text{blank}}}{\text{abs}_{\text{control}}\text{-abs}_{\text{blank}}} \times 100\%.$$

The significance of the particle size, charge, and protein corona types was analyzed by the two-tailed t-test with type 1 grouping.

C. Flow cytometry

For flow cytometry experiments, 3.0×10^5 cells were seeded into individual wells in six-well plate and incubated for 24 h. The cells were rinsed with PBS and DMEM prior to adding PS nanoplastic or PS/protein corona complexes, allowing a further 18 h of incubation. The cells were then rinsed with PBS and collected by adding trypsin/EDTA. Once the detachment of the cells is confirmed, trypsin/EDTA solution was removed by centrifugation. Finally, the cells were suspended in DMEM for the flow cytometry experiment. Data were collected using a three laser Cytek Aurora instrument (Cytek Biosciences, USA). FSC/SSC was used to detect changes in FITC autofluorescence signals of A549 cells. For all data sets presented 100,000 events were shown. Data were analyzed using the FCS Express 7 Research (De Novo Software Inc., USA).

D. Formation of PS/protein corona complexes

The complex was formed by mixing the equal parts of PS nanoplastics and proteins at desirable concentrations dispersed in Tris (10 mM) buffer with NaOH (10 mM) at *p*H 7.4, or in DMEM without FBS. The complexes were equilibrated for a minimum of 30 min.

E. Formation of tethered lipid bilayer

Silicon wafers were cleaned with O_3 for 10 min and rinsed thoroughly with ultrapure water (18.2 MΩ) and ethanol. The freshly cleaned Si wafers were then coated with Cr and Au layers using a magnetron sputter coater with Ar gas as a carrier gas. For EIS, the Cr layer, generated by radio frequency (RF) plasma (30 W), was deposited for 5 min, followed by the Au layer (100 W) for 3 min, resulting in Cr and Au layer thicknesses of approximately 5 and 40 nm, respectively. For NR experiments, Cr and Au were both sputter coated on a 4-in. wafer at 100 W for ∼6 and ∼8 min, respectively.

The Cr/Au coated substrates were cleaned with ethanol and immersed in a DPhyTL and *β*ME ethanolic solution (0.1 mM) with a molar ratio of 8:2 for a minimum of 18 h, allowing the monolayer formation of tethers. The substrates were removed from the tether solution and the excess was washed off with ethanol and dried under a stream of N_2 gas. The second, phospholipid layer was completed using a rapid solvent exchange method.[51] The substrate surface was covered with an ethanolic solution of POPC/cholesterol at a 9:1 molar ratio (10 mM) for 15 min and rapidly rinsed off with an excess an aqueous tris buffer (minimum of five times the cell volume used).

F. Electrochemical impedance spectroscopy

EIS measurements were carried out on a CHI 660E electrochemical station (CH Instruments, Inc.). Spectra were recorded from 150 kHz to 3 mHz at 0 V bias potential, with a 10 mV AC modulation amplitude. A three-electrode system was used, which consisted of a Pt wire (Sigma, Australia) counter electrode coiled around the Ag/AgCl reference electrode (eDAQ Pty Ltd, NSW, Australia), with the Au layer on the substrate acting as the working electrode. An in-house built EIS cell with six wells was used. Individual EIS measurements were conducted in each well, and the spectra were normalized to the area of the well (0.33 cm^2). Nanoplastics, proteins, or nanoplastic/protein complex added to the lipid bilayers were incubated for a minimum of 3.0 h prior to data collection. EIS data were analyzed with a fitting software, ZVIEW (version 3.5c, Scribner Associates, Southern Pine, NC). An equivalent circuit that consisted of resistor and constant phase elements [shown in Fig. 8(d)] was used to fit the EIS spectra between 15 kHz and 0.10 Hz.

G. Neutron reflectometry

NR experiments were conducted on PLATYPUS, time-of-flight reflectometer at Australian Centre for Neutron Scattering (ACNS), Australian Nuclear Science and Technology Organisation (ANSTO), Sydney.[52] Three incident angles, 0.5°, 2°, and 6°, were used to cover the Q-range between 0.005 and 0.4 $Å^{-1}$ by using neutron wavelengths ranging from 2.5 to 19.0 Å. Reflectivity profiles for each sample were collected under D_2O and, where available, CM4.5 (nSLD = 4.5×10^{-6} $Å^{-2}$). The tethered lipid bilayers were exposed to PS nanoplastics, proteins, or nanoplastics/protein complexes after collecting the reflectivity profile of the control bilayers.

NR data reduction and analysis were performed on REFNX reflectometry analysis package.[53] A slab layer model was used to fit and corefine (where a second solvent was available) the reflectivity profiles. Four parameters were used to describe a slab layer: thickness, nSLD, roughness, and solvent volume fraction. The roughness values of all slab layers were linked to the interfacial roughness of the Au layer to reduce the number of fitting parameters (global roughness). The fitting model did not consider cholesterol as an independent slab and assumed it to be embedded in the hydrophobic chains. Markov-chain Monte Carlo error analysis was used to estimate the uncertainties of fitted values.[53]

ACKNOWLEDGMENTS

S.K. would like to acknowledge the University of Auckland (Award: doctoral scholarship) and AINSE Ltd. (Award: postgraduate scholarship) for commencing the doctoral work. We would also like to acknowledge ANSTO for providing the PLATYPUS neutron reflectometry beamtime (Nos. P7307 and P7390). We would also like to thank John Taylor from the University of Auckland for generously sharing his A549 cells.

DATA AVAILABILITY

The data that support the findings of this study are available from the corresponding author upon reasonable request.

REFERENCES

[1]J. R. Jambeck, R. Geyer, C. Wilcox, T. R. Siegler, M. Perryman, A. Andrady, R. Narayan, and K. L. Law, Science **347**, 768 (2015).
[2]E. J. Carpenter and K. Smith, Science **175**, 1240 (1972).
[3]W. J. Veneman, H. P. Spaink, N. R. Brun, T. Bosker, and M. G. Vijver, Aquat. Toxicol. **190**, 112 (2017).

[4]World Health Organisation (WHO), "Microplastics in drinking-water;" 2019. See https://www.who.int/water_sanitation_health/publications/microplastics-in-drinking-water/en/
[5]"Microplastics expert workshop report; EPA office of wetlands, oceans and watersheds: America," 2017. See: https://www.epa.gov/trash-free-waters/microplastics-expert-workshop-report#:~:text=Microplastics%20Expert%20Workshop%20Report,to%20human%20and%20ecological%20health
[6]Office of the Prime Minister's Chief Science Advisor, New Zealand, "Rethinking plastics in Aotearoa New Zealand," December 2019. See https://www.pmcsa.ac.nz/topics/rethinking-plastics/
[7]B. Koelmans *et al.*, *A Scientific Perspective on Microplastics in Nature and Society* (SAPEA, Brussels, 2019).
[8]L. C. Peng, D. D. Fu, H. Y. Qi, C. Q. Lan, H. M. Yu, and C. J. Ge, Sci. Total Environ. **698**, 134254 (2020).
[9]L. Rubio, R. Marcos, and A. Hernandez, J. Toxicol. Environ. Health, Part B **23**, 51 (2020).
[10]M. C. Shen, Y. X. Zhang, Y. Zhu, B. Song, G. M. Zeng, D. F. Hu, X. F. Wen, and X. Y. Ren, Environ. Pollut. **252**, 511 (2019).
[11]P. Wick *et al.*, Environ. Health Perspect. **118**, 432 (2010).
[12]L. Bradney, H. Wijesekara, K. N. Palansooriya, N. Obadamudalige, N. S. Bolan, Y. S. Ok, J. Rinklebe, K. H. Kim, and M. B. Kirkham, Environ. Int. **131**, 104937 (2019).
[13]P. Stapleton, AIMS Environ. Sci. **6**, 367 (2019).
[14]S. Kihara, I. Köper, J. P. Mata, and D. J. McGillivray, Adv. Colloid Interface Sci. **288**, 102337 (2021).
[15]K. Mattsson, E. V. Johnson, A. Malmendal, S. Linse, L.-A. Hansson, and T. Cedervall, Sci. Rep. **7**, 11452 (2017).
[16]Z. Liu, P. Yu, M. Cai, D. Wu, M. Zhang, Y. Huang, and Y. Zhao, Chemosphere **215**, 74 (2019).
[17]Z. Q. Liu, M. Q. Cai, D. L. Wu, P. Yu, Y. Jiao, Q. C. Jiang, and Y. L. Zhao, Environ. Pollut. **256**, 113506 (2020).
[18]W. Lin, R. F. Jiang, S. Z. Hu, X. Y. Xiao, J. Y. Wu, S. B. Wei, Y. X. Xiong, and G. F. Ouyang, Ecotoxicol. Environ. Saf. **180**, 509 (2019).
[19]P. M. Gopinath *et al.*, Sci. Rep. **9**, 8860 (2019).
[20]M. Hesler *et al.*, Toxicol. In Vitro **61**, 104610 (2019).
[21]T. A. Qiu, P. L. Clement, and C. L. Haynes, ChemComm **54**, 12787 (2018).
[22]S. Kihara, N. J. van der Heijden, C. K. Seal, J. P. Mata, A. E. Whitten, I. Köper, and D. J. McGillivray, Bioconjugate Chem. **30**, 1067 (2019).
[23]D. Walczyk, F. B. Bombelli, M. P. Monopoli, I. Lynch, and K. A. Dawson, J. Am. Chem. Soc. **132**, 5761 (2010).
[24]A. Lesniak, F. Fenaroli, M. P. Monopoli, C. Åberg, K. A. Dawson, and A. Salvati, ACS Nano **6**, 5845 (2012).
[25]C. C. Fleischer and C. K. Payne, J. Phys. Chem. B **118**, 14017 (2014).
[26]F. Barbero *et al.*, Semin. Immunol. **34**, 52 (2017).
[27]S. Kihara, S. Ghosh, D. R. McDougall, A. Whitten, J. Mata, I. Köper, and D. J. McGillivray, Biointerphases **15**, 051003 (2020).
[28]B. Raguse, V. Braach-Maksvytis, B. A. Cornell, L. G. King, P. D. J. Osman, R. J. Pace, and L. Wieczorek, Langmuir **14**, 648 (1998).
[29]R. Naumann *et al.*, Langmuir **19**, 5435 (2003).
[30]F. Heinrich, T. Ng, D. J. Vanderah, P. Shekhar, M. Mihailescu, H. Nanda, and M. Losche, Langmuir **25**, 4219 (2009).
[31]S. Kihara, S. Ghosh, D. R. McDougall, A. E. Whitten, J. P. Mata, I. Köper, and D. J. McGillivray, Biointerphases **15**, 051002 (2020).
[32]R. Foldbjerg, D. A. Dang, and H. Autrup, Arch. Toxicol. **85**, 743 (2011).
[33]H. Suzuki, T. Toyooka, and Y. Ibuki, Environ. Sci. Technol. **41**, 3018 (2007).
[34]J. Andersson, M. A. Fuller, K. Wood, S. A. Holt, and I. Köper, Phys. Chem. Chem. Phys. **20**, 12958 (2018).
[35]J. Andersson and I. Köper, Membranes **6**, 30 (2016).
[36]J. J. Knobloch, A. R. Nelson, I. Köper, M. James, and D. J. McGillivray, Langmuir **31**, 12679 (2015).
[37]Q. Chen, M. Gundlach, S. Yang, J. Jiang, M. Velki, D. Yin, and H. Hollert, Sci. Total Environ. **584**, 1022 (2017).
[38]L.-J. Feng *et al.*, Environ. Sci. Technol. **54**, 3386 (2020).
[39]M. Prüst, J. Meijer, and R. H. Westerink, Part. Fibre Toxicol. **17**, 1 (2020).
[40]C. Cortés, J. Domenech, M. Salazar, S. Pastor, R. Marcos, and A. Hernández, Environ. Sci. Nano **7**, 272 (2020).
[41]A. Albanese and W. C. W. Chan, ACS Nano **5**, 5478 (2011).
[42]S. Bakand, A. Hayes, and F. Dechsakulthorn, Inhalation Toxicol. **24**, 125 (2012).
[43]V. Mirshafiee, R. Kim, S. Park, M. Mahmoudi, and M. L. Kraft, Biomaterials **75**, 295 (2016).
[44]N. Duran, C. P. Silveira, M. Duran, and D. S. T. Martinez, J. Nanobiotechnol. **13**, 55 (2015).
[45]B. Kharazian, N. L. Hadipour, and M. R. Ejtehadi, Int. J. Biochem. Cell Biol. **75**, 162 (2016).
[46]D. Di Silvio, M. Maccarini, R. Parker, A. Mackie, G. Fragneto, and F. Baldelli Bombelli, J. Colloid Interface Sci. **504**, 741 (2017).
[47]S. Burgess, Z. J. Wang, A. Vishnyakov, and A. V. Neimark, J. Colloid Interface Sci. **561**, 58 (2020).
[48]C. M. Beddoes, C. P. Case, and W. H. Briscoe, Adv. Colloid Interface Sci. **218**, 48 (2015).
[49]A. Pitchaimani, N. Tuyen Duong Thanh, M. Koirala, Y. Zhang, and S. Aryal, Toxicol. In Vitro **43**, 29 (2017).
[50]Y. N. Wu, F. Li, W. Zhu, J. Cui, C. A. Tao, C. Lin, P. M. Hannam, and G. Li, Angew. Chem. **123**, 12726 (2011).
[51]B. A. Cornell, V. Braach-Maksvytis, L. King, P. Osman, B. Raguse, L. Wieczorek, and R. Pace, Nature **387**, 580 (1997).
[52]M. James, A. Nelson, S. Holt, T. Saerbeck, W. Hamilton, and F. Klose, Nucl. Instrum. Methods Phys. Res., Sect. A **632**, 112 (2011).
[53]A. R. Nelson and S. W. Prescott, J. Appl. Crystallogr. **52**, 193 (2019).
[54]See supplementary material at https://www.scitation.org/doi/suppl/10.1116/6.0001124 for additional flow cytometry, florescence microscopy, EIS, and NR data.